Phase-matching condition for THz wave generation via difference frequency generation using InxGa1-xSe mixed crystals

Phase-matching condition for THz wave generation via difference frequency generation using In$_x$Ga$_{1-x}$Se mixed crystals

YOHEI SATO,[1,*] ⓘ MAYU NAKAJIMA,[1] CHAO TANG,[1] ⓘ KATSUYA WATANABE,[1] TADAO TANABE,[1,2] AND YUTAKA OYAMA[1]

[1]*Department of Materials Science and Engineering, Tohoku University, Miyagi 980-8579, Japan*
[2]*Present address: Department of Engineering and Design, Shibaura Institute of Technology 3-9-14 Shibaura, Minato-ku, Tokyo 108-8548, Japan*
*s.yohei1662@gmail.com

Abstract: Terahertz (THz) waves at 9.7, 10.1 and 10.6 THz were generated via difference frequency generation in high-quality In$_x$G$_{1-x}$aSe mixed crystals with a relatively high indium compositions ($x = 0.040, 0.048, 0.074$) grown from an indium flux. The phase-matching angle for THz wave generation was measured for each indium content. As a result, it is confirmed that the incident angle of the excitation light satisfying the phase-matching condition is shifted to a higher angle with an increase in the indium content.

1. Introduction

Gallium selenide (GaSe) is one of the most promising layered chalcogenide semiconductors for future novel optoelectronic devices. In its 2 dimensional (2D) form, GaSe has attractive electrical and optical characteristics originating from the finite energy band gap and has been studied and developed for a variety of devices such as THz wave light sources [1–4] and spin-field-effect transistors [5].

GaSe has an extremely asymmetric layered crystal structure, which leads to a relatively high second order nonlinear optical (NLO) constant ($d_{22} = 54$ pm/V) [6]. Therefore, efficient THz waves can be generated in GaSe crystals via the difference frequency generation (DFG) method, which relies on second order NLO effects. In addition, GaSe crystals are transparent over a wide range from infrared (IR) to THz frequencies and it is possible, theoretically, to generate THz waves from the THz to mid-IR (0.1 ~ 100 THz) via DFG [1–4]. Furthermore, layered 2D semiconductor GaSe crystals have a high birefringence, making it possible to apply collinear phase matching when generating THz waves via DFG with the possibility of improving the conversion coefficient [7–9].

However, because the growth of GaSe tends to be extremely anisotropic, stacking faults are easily generated in the crystal making it difficult to grow material of high optical quality [10]. These issues arise because the inter-layers of GaSe are weakly bound by van der Waals bonding forces even though the intra-layer atoms are strongly bonded by covalent bonding forces. The van der Waals bonding forces involved were described theoretically by London in 1937 [11]. Our group has directly measured these in order to obtain a crucial understanding of this layered semiconductor crystal and to understand how to strengthen the inter-layer van der Waals bonding force [12]. Finally, due to their poor mechanical properties, it is problematic to cut or polish GaSe crystals in order that they can be used as light sources.

In previous studies, attempts have been made to solve these problems by doping GaSe with various elements such as S [13,14], Te [15,16], In, Al [17], Er [18], Ti [19] and Ge [20]. The reports of doped GaSe crystals are reviewed in Ref. [21]. In particular, the microhardness of GaSe crystal was observed to be increased by doping of indium [22,23]. In addition, improvements in

the second order NLO constant in second-harmonic generation (SHG) [23,24] and the conversion efficiency for generating THz waves by DFG [25] has been also been reported. However, although there have been reports on improving the NLO properties of GaSe crystals by doping them with indium, changes in phase-matching conditions due to doping with indium has not yet been confirmed because of the relatively low indium compositions of $In_xGa_{1-x}Se$ ($x = 0.001–0.030$) crystal found in the GaSe crystals previously produced [23,26].

In this study, high quality $In_xGa_{1-x}Se$ mixed crystals with relatively high indium composition were grown by solution growth from indium flux. THz wave generation was then performed on the $In_xGa_{1-x}Se$ ($x = 0.040, 0.048, 0.074$) crystals via difference frequency generation. Additionally, the relationship between the phase-matching conditions and the indium composition was confirmed by measuring the incident angle of the pump light which generates the maximum output of the THz wave for each indium composition and the change of the phase-matching angle due to the doping with indium was considered from the refractive index.

2. Experiments

$In_xGa_{1-x}Se$ mixed crystals were grown by the traveling heater method (THM). 7.7 g of indium (DOWA Electronics Materials Co., Ltd.) was used as a solvent and 20g of polycrystals of GaSe (Kojundo Chemical Lab. Co., Ltd.) were used as a source material. The purity of the GaSe and indium were 3N and 6N, respectively. In this work, the $In_xGa_{1-x}Se$ mixed crystals were grown by THM at three different growth temperatures. In the THM, the growth speed can be controlled by the speed of the growth vessel or heater. The growth temperature was defined by the temperature at the starting position before the pulling of the growth vessel and these were about 700 °C, 740 °C, 780 °C. The growth process is as follows: first, the growth vessel was fixed at the initial position and homogenization occurred in the In-Ga-Se solution by diffusion of the Ga and Se to the bottom of the crucible due to the concentration gradient. The growth vessel was kept at this initial position for 1 day at the growth temperature for 700 and then 780 °C and for 7 days at the growth temperature of 740 °C. After the homogenization, the growth vessel was mechanically lowered at a speed of 60 µm/hour for 21 days at the growth temperature of 700 and 780 °C and for 14 days in the condition of growth temperature of 740 °C. The heating up rate to the temperature shown in Fig. 1 was 20 °C/min and the cooling down rate to room temperature was 1°C/min.
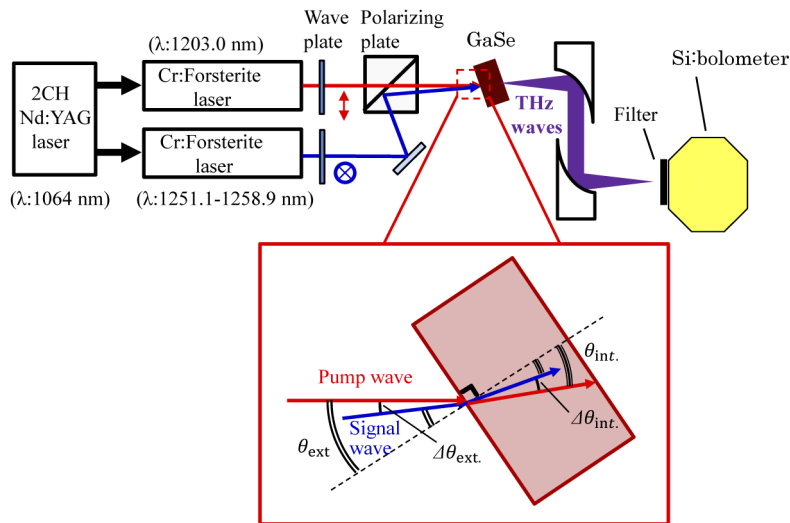

Fig. 1. Schematic view of the THz wave generation system and definition of angles of excitation light

Electron probe micro-analysis (EPMA) was used to measure the indium content in the grown crystals using a Field Emission Scanning Electron Microscope (FE-SEM) (JXA-8530F, JEOL Ltd.). Measurements were also made of reference samples of undoped GaSe crystals grown by TDM-CVP [8] and an undoped InP wafer (Sumitomo electric industries, Ltd.). The indium content was measured at 7 points on each sample. We calculated the average and standard deviation of these 7 points. In addition, we also estimated the indium content in the grown crystal from the lattice constants measured by XRD measurements, based on the change in lattice constant due to indium doping. Symmetric X-ray diffraction patterns of $In_xGa_{1-x}Se$ mixed crystals from (0 0 14) to (0 0 20) were measured using an automated multipurpose X-ray diffractometer (SmartLab, RIGAKU Ltd) with $CuK\alpha_1$ (λ=0.154056 nm) radiation. The precise lattice constant was estimated by extrapolating to $\cos^2\theta = 0$ on a plot of $\cos^2\theta$ vs. the lattice constant c.

THz waves were generated via difference frequency generation from the $In_xGa_{1-x}Se$ mixed crystals grown in this study and an undoped GaSe crystal (Altechna Co. Ltd.) at room temperature. The surface was treated by a tape peeling method. The optical system for generating the THz waves is shown in Fig. 2. A near-infrared Nd:YAG laser (LOTIIS Inc.) with two channels was used to excite grating type Cr:Foresterite lasers. These lasers, which have gratings (1200 grooves/mm) for wavelength selection achieve a higher-frequency purity than prism type ones. In this study, THz waves were generated at 9.7, 10.1 and 10.6 THz by *eoo* collinear phase-matching conditions. The wavelength of the pump light (extra-ordinary light) was1203.0 nm and the signal light (ordinary light) were 1251.6, 1253.7 and 1256.3 nm for the THz wave generation at 9.7, 10.1 and 10.6 THz, respectively. The pulse width and repetition frequency were 12 ns and 10 Hz, respectively. The pulse energy of pump light and signal light were 1.5 mJ. The signal and pump light were incident on the (001) face of the $In_xGa_{1-x}Se$ crystal and propagated coaxially in the crystal under perfect phase-matching conditions. The diameter of aluminum aperture in Fig. 1 was 3 mm. Phase-matching conditions were achieved by changing the angle at which the excitation light was incident on the crystal. The THz waves were detected by a 4K-Si:Bolometer (Infrared Inc.). The NIR excitation light was safely removed by means of black polyethylene placed in front of the Si:Bolometer.
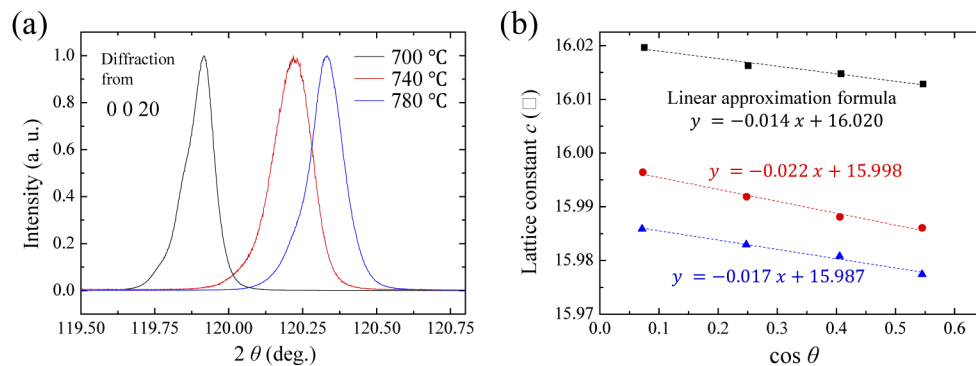

Fig. 2. (a) X-ray diffraction peaks from (0 0 18), (b) The plot of $\cos^2\theta$ vs. the lattice constant c calculated from diffraction peak from (0 0 14) to (0 0 20)

The position of the crystals used for THz wave generation and the polarizing plate are shown in Fig. 1 were placed on a horizontally rotatable rotary stage. The rotation steps of the crystal and polarizing plate were 0.05 and 0.1 °, respectively. As shown in Fig. 1, the incident angle of the pump light to the crystal θ_{ext} can be controlled by rotation of the crystal and the incident angle of signal light can be controlled by the rotation of the crystal and the polarizing plate. The crystal rotation angle of 0 ° was defined as the angle of crystal where the pump light was normally

incident on the (001) surface. The crystal rotation angle of 0 ° was adjusted by matching the position of the reflected pump light from the crystal with the position of the incident light at the wave plate. In this study, the phase-matched peak was confirmed by the relationship between the THz wave intensity and rotation angle of the crystal under the conditions of the polarizer angle at which the THz wave intensity was maximized.

3. Results and discussion

3.1. Indium content in the grown crystal by EPMA and XRD

Using EPMA, the average indium contents of grown crystals at 700 °C, 740 °C and 780 ∘C were obtained as 3.7 at%, 2.4 at% and 2.0 at%, respectively, where the standard deviations are 0.0012 at%, 0.0003 at% and 0.011 at%. Figure 3(a) shows the XRD peaks from (0 0 20), and Fig. 3(b) shows a plot of $\cos^2\theta$ vs. the lattice constant c calculated using the XRD peaks from (0 0 14), (0 0 16), (0 0 18) and (0 0 20). As shown in Fig. 3(b), the estimated c lattice constants of the grown crystal at 700 °C, 740 °C and 780 °C were 16.020 Å, 15.998 Å and 15.987 Å, respectively. According to Vegard's law and considering the lattice constants for GaSe ($c = 15.95$Å) and InSe ($c = 16.70$ Å) [27], the indium content in the grown crystals at 700 °C, 740 °C and 780 °C was calculated as 4.67 at%, 3.20 at% and 2.47 at% from the lattice constants 16.020 Å, 15.998 Å and 15.987 Å, respectively. The indium contents estimated by XRD measurements are similar to the values measured by EPMA. Therefore, we believe that the $In_xGa_{1-x}Se$ mixed crystal was grown from indium flux and that the indium atoms were substituted at Ga sites. The above results of EPMA and XRD were previously reported in Ref. [28].

3.2. Phase-matching condition of THz wave generation

Figures 3(a), (b) and (c) show the phase-matched peaks at 9.7, 10.1 and 10.6 THz in the relationship between the THz wave intensity and incident angle of pump light for each indium content. The details of samples used for THz wave generation are shown in Table 1. The conversion efficiency was calculated from pulse energies of excitation lights and THz wave shown in Table 2 as follows.

$$\text{Conversion efficiency (J}^1\text{)} = \frac{P_{THz}\ (\text{J})}{P_{pump}(\text{J}) \cdot\ P_{signal}\ (\text{J})}. \tag{1}$$

The maximum conversion efficiency of each indium content and THz wave frequency is shown in Table 3. As shown in Fig. 3, the phase-matched peaks shift to the higher incident angle side of the pump light with an increase in the indium content. In order to confirm the relationship between the position of the phase-matched peak and the indium content, the fitting curve of the measured phase-matching peak was calculated and the center position of the peak $\theta_{\text{ext.}}^{\text{fit. (pump)}}$ was determined from of the following considerations.

Table 1. Indium content and thickness of the crystal used for THz wave generation

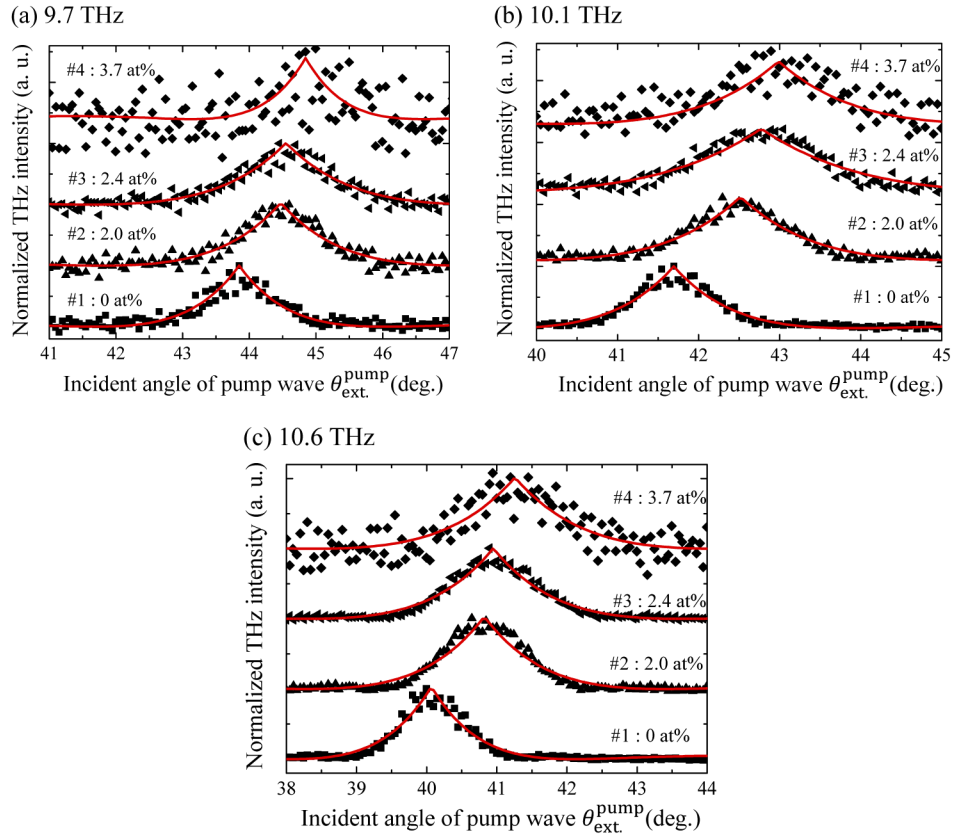| Sample number	Growth temperature (°C)	In content (at%)	Thickness (μm)
1		0	1021
2	780	2.0	860
3	740	2.4	790
4	700	3.7	1200

(a) 9.7 THz

(b) 10.1 THz

(c) 10.6 THz

Fig. 3. Phase-matched peak at (a) 9.7 THz, (b) 10.1 THz and (c) 10.6 THz in the THz wave generation from 4 samples with different In content. Here black squares are the measured points and the solid red line are the fitting curve

Table 2. The THz pulse energy of each indium content and THz wave frequency

In content (at%)	9.7 THz	10.1 THz	10.6 THz
0	140 pJ	410 pJ	470 pJ
2.0	98 pJ	180 pJ	220 pJ
2.4	77 pJ	120 pJ	230 pJ
3.7	14 pJ	25 pJ	24 pJ

Table 3. The maximum conversion efficiency of each indium content and THz wave frequency

In content (at%)	9.7 THz	10.1 THz	10.6 THz
0	6.1×10^{-5} J^{-1}	1.7×10^{-4} J^{-1}	2.0×10^{-4} J^{-1}
2.0	4.2×10^{-5} J^{-1}	7.7×10^{-5} J^{-1}	9.5×10^{-5} J^{-1}
2.4	3.3×10^{-5} J^{-1}	5.3×10^{-5} J^{-1}	9.6×10^{-5} J^{-1}
3.7	6.0×10^{-6} J^{-1}	1.1×10^{-5} J^{-1}	1.0×10^{-5} J^{-1}

THz wave intensity obtained using DFG is given by [29]

$$I_{\text{THz}}(L) = \frac{2\,I_{\text{pump}}I_{\text{signal}}d_{\text{eff}}{}^2\omega_{\text{THz}}{}^2}{n_{\text{pump}}n_{\text{signal}}n_{\text{THz}}\varepsilon_0 c^3}L^2\text{sinc}^2\left(\frac{\Delta kL}{2}\right) \times T_{\text{pump}}T_{\text{signal}}T_{\text{THz}}$$
$$\times e^{-\alpha_{\text{THz}}L}\frac{1 + e^{-\alpha_{\text{THz}}L} - 2e^{-\frac{1}{2}\Delta\alpha L}}{\left(\frac{1}{2}\Delta\alpha L\right)^2} \qquad , \qquad (2)$$

where I_{pump}, I_{signal} and I_{THz} are the output power of the pump light, the signal light and the THz waves generated via DFG, respectively, $d_{\text{eff}} = -d_{22}\cos\,\theta_{\text{int.}}\sin\,3\varphi$ is the effective NLO coefficient [30], $\theta_{\text{int.}}$ is the internal phase-matching angle and φ is the azimuthal angle, ω_{THz} is the angular frequency of the THz waves, n is the refractive index, T is the transmittance at the crystal surface, α is the absorption coefficient ($\Delta\alpha = \alpha_{\text{pump}} + \alpha_{\text{signal}} - \alpha_{\text{THz}}$), L is the interaction length of the pump and signal light in the crystal, Δk is wave vector mismatch. Because the center position and the shape of phase-matched peak heavily depends on L and Δk, the fitting curve was calculated using including only L and Δk as variables. Additionally, L, which influences the peak width and the maximum value, is not used as a value calculated from the crystal thickness, but is used as a parameter adjusted to minimize the error between the measured value and the calculated value, since the normalized measured value was fitted by the normalized calculated value.

$$I_{\text{THz}} = L^2\text{sinc}^2\left(\frac{\Delta kL}{2}\right) \qquad (3)$$

As shown in Fig. 1, Δk depends on the difference of the propagation angle $\Delta\theta_{\text{int.}}$ between the pump light and signal light in the crystal and absolute value of wave vector of pump light, signal light and the THz wave. Therefore, Δk is expressed by

$$\Delta k = \sqrt{|k_{\text{THz}}|^2 - (|k_{\text{pump}}|^2 + |k_{\text{signal}}|^2 - 2|k_{\text{pump}}||k_{\text{signal}}|\cos\Delta\theta_{\text{int.}})}. \qquad (4)$$

In the case of Fig. 1, when Δk is equal to 0 at the optimum incident angle of the pump light and the signal light, the THz wave with the maximum intensity is generated by collinear phase matching and $\Delta\theta_{\text{int.}}$ is equal to 0. Therefore, if $\Delta\theta_{\text{int.}}$ is the minimum value, the Δk calculated from Eq. (4) becomes the minimum value. Although k can be obtained using Sellmeier's dispersion formula [6], the center of fitting curve deviates from the center of the measured phase-matched peak because the Δk obtained using Sellmeier's dispersion formula does not represent the minimum value when $\Delta\theta_{\text{int.}}$ is the minimum value. In order to match the center of fitting curve and measured peak, k_{THz} is substituted to $(k_{\text{pump}}^{\text{fit.}} - k_{\text{signal}})$ in Eq. (4), where $k_{\text{pump}}^{\text{fit.}}$ is the wave number of the pump light when the incident angle is equal to the value of the center position of the fitting curve. Equation (4) is modified as follows by substituting k_{THz} to $(k_{\text{pump}}^{\text{fit.}} - k_{\text{signal}})$.

$$\Delta k = \sqrt{|k_{\text{pump}}^{\text{fit.}} - k_{\text{signal}}|^2 - (|k_{\text{pump}}|^2 + |k_{\text{signal}}|^2 - 2|k_{\text{pump}}||k_{\text{signal}}|\cos\Delta\theta_{\text{int.}})} \qquad (5)$$

Regardless of the propagation direction in the crystal, the wave vector of signal light, which is the ordinary light is expressed by:

$$k_{\text{signal}} = 2\pi/\lambda_{\text{signal}} = n_{\text{signal}}\omega_{\text{signal}}/c \qquad (6)$$

where ω is the angular frequency. On the other hand, the wave vector of pump light, which is the extra-ordinary light depends on the propagation direction in the crystal and is expressed by:

$$
\begin{aligned}
k_{\text{pump}} &= 2\pi/\lambda_{\text{pump}} = n_{\text{pump}}\omega_{\text{pump}}/c \\
&= \left(\sqrt{\frac{\sin^2\theta_{\text{int.}}^{\text{pump}}}{n_{\text{e}\perp}^2} + \frac{\cos^2\theta_{\text{int.}}^{\text{pump}}}{n_{\text{o}}^2}} \right)^{-1} \times \frac{\omega_{\text{pump}}}{c} \\
&= \frac{\omega_{\text{pump}}}{c} \sqrt{n_{\text{o}}^2 \times \left(1 - \frac{\sin^2\theta_{\text{ext.}}^{\text{pump}}}{n_{\text{e}\perp}^2} + \frac{\sin^2\theta_{\text{ext.}}^{\text{pump}}}{n_{\text{o}}^2} \right)}
\end{aligned}
\tag{7}
$$

where the refractive indices n, $n_{\text{e}\perp}$ and n_{o} are obtained using Sellmeier's dispersion formula [6] and $\theta_{\text{ext.}}^{\text{pump}}$ is the incident angle of pump light. $k_{\text{pump}}^{\text{fit.}}$ can be calculated by substituting $\theta_{\text{ext.}}^{\text{pump}}$ to $\theta_{\text{ext.}}^{\text{fit. (pump)}}$ in Eq. (7), where $\theta_{\text{ext.}}^{\text{fit. (pump)}}$ is the value of the center angle of the fitting curve.

In Eq. (5), $\Delta\theta_{\text{int.}}$ is expressed by

$$
\Delta\theta_{\text{int.}} = \theta_{\text{int.}}^{\text{pump}} - \theta_{\text{int.}}^{\text{signal}}
\tag{8}
$$

where $\theta_{\text{int.}}^{\text{pump}}$ is expressed by

$$
\theta_{\text{int.}}^{\text{pump}} = \arcsin\left[\frac{\sin\theta_{\text{ext.}}^{\text{pump}}}{n_{\text{pump}}} \right] = \arcsin\left[\frac{\sin\theta_{\text{ext.}}^{\text{pump}}}{\sqrt{n_{\text{o}}^2 \times \left(1 - \frac{\sin^2\theta_{\text{ext.}}^{\text{pump}}}{n_{\text{e}\perp}^2} + \frac{\sin^2\theta_{\text{ext.}}^{\text{pump}}}{n_{\text{o}}^2} \right)}} \right]
\tag{9}
$$

In addition, since $\Delta\theta_{\text{ext.}}$ in Fig. 1 does not change during the measurement of the phase-matched peak, $\theta_{\text{int.}}^{\text{signal}}$ is expressed as follows by using $\Delta\theta_{\text{ext.}}$:

$$
\begin{aligned}
\theta_{\text{int.}}^{\text{signal}} &= \arcsin\left[\frac{\sin\{\theta_{\text{ext.}}^{\text{signal}}\}}{n_{\text{signal}}} \right] = \arcsin\left[\frac{\sin\{\theta_{\text{ext.}}^{\text{pump}} - \Delta\theta_{\text{ext.}}\}}{n_{\text{signal}}} \right] \\
&= \arcsin\left[\frac{\sin\{\theta_{\text{ext.}}^{\text{pump}} - (\theta_{\text{ext.}}^{\text{fit. (pump)}} - \theta_{\text{ext.}}^{\text{fit. (signal)}})\}}{n_{\text{signal}}} \right] \\
&= \arcsin\left[\frac{\sin\{\theta_{\text{ext.}}^{\text{pump}} - (\theta_{\text{ext.}}^{\text{fit. (pump)}} - \arcsin(n_{\text{signal}}\sin\theta_{\text{int.}}^{\text{fit. (signal)}}))\}}{n_{\text{signal}}} \right]
\end{aligned}
\tag{10}
$$

where $\theta_{\text{int.}}^{\text{fit. (signal)}}$ is the propagation angle of the signal light in the crystal when the phase-matched condition is satisfied. Because collinear phase matching is satisfied in the crystal when the incident angle of pump light and signal light are in the optimal condition, $\theta_{\text{int.}}^{\text{fit. (signal)}}$ is equal to $\theta_{\text{int.}}^{\text{fit. (pump)}}$. Therefore, $\theta_{\text{int.}}^{\text{signal}}$ is expressed as follows by modifying Eq. (10):

$$
\begin{aligned}
\theta_{\text{int.}}^{\text{signal}} &= \arcsin\left[\frac{\sin\{\theta_{\text{ext.}}^{\text{pump}} - (\theta_{\text{ext.}}^{\text{fit. (pump)}} - \arcsin(n_{\text{signal}}\sin\theta_{\text{int.}}^{\text{fit. (pump)}}))\}}{n_{\text{signal}}} \right] \\
&= \arcsin\left[\frac{\sin\left\{\theta_{\text{ext.}}^{\text{pump}} - \left(\theta_{\text{ext.}}^{\text{fit. (pump)}} - \arcsin(n_{\text{signal}}\Delta\frac{\sin\theta_{\text{ext.}}^{\text{fit. (pump)}}}{n_{\text{pump}}^{\text{fit.}}})\right)\right\}}{n_{\text{signal}}} \right]
\end{aligned}
\tag{11}
$$

where $n_{\text{pump}}^{\text{fit.}}$ is expressed by

$$n_{\text{pump}}^{\text{fit.}} = \sqrt{n_{\text{o}}^2 \times \left(1 - \frac{\sin^2\theta_{\text{ext.}}^{\text{fit. (pump)}}}{n_{\text{e}\perp}^2} + \frac{\sin^2\theta_{\text{ext.}}^{\text{fit. (pump)}}}{n_{\text{o}}^2}\right)}. \tag{12}$$

From the above, the fitting curve is calculated using Eqs. (3), (5)–(9), (11) and (12). Using the above equations, the normalized THz intensity can be obtained from the incident angle of the pump light $\theta_{\text{ext.}}^{\text{pump}}$. In the above equations, the center position of the phase-matched peak $\theta_{\text{ext.}}^{\text{fit. (pump)}}$ is determined by adjusting $\theta_{\text{ext.}}^{\text{fit. (pump)}}$ and L so that the difference between the measured value and the calculated value is minimized.

For the THz wave generation at 9.7, 10.1 and 10.6 THz, the center positions of the phase-matched peak $\theta_{\text{ext.}}^{\text{fit. (pump)}}$. were obtained for each indium content by fitting the measured values and the relationship between the center position and the indium content is shown in Fig. 4. As shown in Fig. 4, the incident angle of the pump light satisfying the phase matching tends to shift to the higher incident angle side of the pump light with an increase of the indium content for THz wave generation at any of the three frequencies. Here, according to the momentum conversion law, the refractive index of the pump light at the phase-matching condition is expressed by:

$$n_{\text{pump}}^{\text{fit.}} = \frac{n_{\text{THz}}\omega_{\text{THz}} + n_{\text{signal}}\omega_{\text{signal}}}{\omega_{\text{pump}}} \tag{13}$$

If the refractive index of the ordinary light did not change, but that of the extra-ordinary light changes with an increase in the indium content the refractive index of the pump light $n_{\text{pump}}^{\text{fit.}}$ satisfying the *eoo* phase-matching condition doenot change with an increase in the indium content according to Eq. (12). Additionally, the extra-ordinary refractive index of the pump light $n_{\text{e}\perp}$ is expressed as follows, by modifying Eq. (12):

$$n_{\text{e}\perp} = \sqrt{\frac{n_{\text{o}}^2}{(n_{\text{o}}^2 - n_{\text{pump}}^{\text{fit.}}{}^2)/\sin^2\theta_{\text{ext.}}^{\text{fit. (pump)}} + 1}} \tag{14}$$
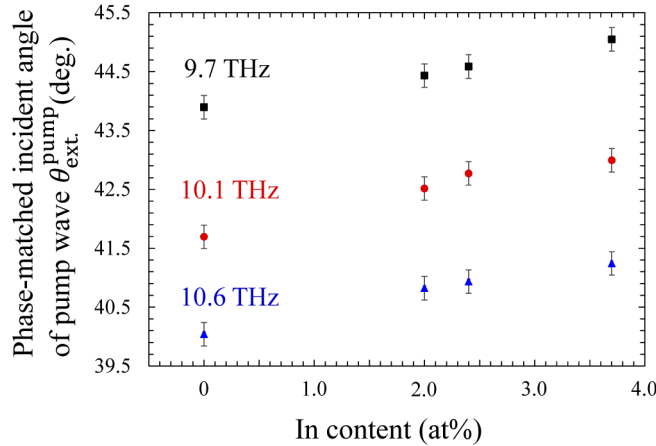

Fig. 4. Relationship between the phase-matched incident angle of pump light and the indium content

According to Eq. (14), because n_{o} and $n_{\text{o}}^2 - n_{\text{pump}}^{\text{fit.}}{}^2$ (>0) are constant values, $n_{\text{e}\perp}$ increases with an increase of $\theta_{\text{ext.}}^{\text{fit. (pump)}}$. Therefore, it is considered that shift of the incident angle of

the pump light toward the higher angle side with an increase in the indium content indicates a reduction of birefringence of $In_xGa_{1-x}Se$ mixed crystal.

4. Summary

We have generated THz waves at 9.7, 10.1 and 10.6 THz via difference frequency generation using an $In_xGa_{1-x}Se$ ($x = 0.04, 0.048, 0.074$) mixed crystal grown from an indium flux. As a result of measurement of the phase-matching angle for each indium content, it is confirmed that the incident angle of the pump light satisfying the phase-matching condition is shifted to a higher angle side with an increase in the indium content. It is considered that this is because the extra-ordinary refractive index of the $In_xGa_{1-x}Se$ mixed crystal decreases with an increase in the indium content.

Funding

Disclosures

The authors declare no conflicts of interest.

References

1. W. Shi, Y. J. Ding, N. Fernelius, and K. Vodopyanov, "Efficient, tunable, and coherent 0.18–5.27-THz source based on GaSe crystal," Opt. Lett. **27**(16), 1454–1456 (2002).
2. W. Shi and Y. Ding, "A monochromatic and high-power terahertz source tunable in the ranges of 2.7–38.4 and 58.2–3540 μm for variety of potential applications," J. Appl. Phys. Lett. **84**(10), 1635–1637 (2004).
3. T. Tanabe, K. Suto, J. Nishizawa, and T. Sasaki, "Characteristics of terahertz-wave generation from GaSe crystals," J. Phys. D: Appl. Phys. **37**(2), 155–158 (2004).
4. K. Saito, Y. Nagai, K. Yamamoto, K. Maeda, T. Tanabe, and Y. Oyama, "Terahertz Wave Generation via Nonlinear Parametric Process from ε-GaSe Single Crystals Grown by Liquid Phase Solution Method," Opt. Photonics J. **04**(08), 213–218 (2014).
5. S. Takasuna, J. Shiogai, S. Matsuzaka, M. Kohda, Y. Oyama, and J. Nitta, "Weak antilocalization induced by Rashba spin-orbit interaction in layered III-VI compound semiconductor GaSe thin films," Phys. Rev. B **96**(16), 161303 (2017).
6. V. G. Dmitriev, G. G. Gurzadyan, and D. N. Nikogosyan, *Handbook of Nonlinear Optical Crystals*. Springer, Berlin, pp. 166–169 (1997).
7. C. W. Chen, T. T. Tang, S. H. Lin, J. Y. Huang, C.-S. Chang, P. K. Chung, S. T. Yen, and C. L. Pan, "Optical properties and potential applications of ε-GaSe at terahertz frequencies," J. Opt. Soc. Am. B **26**(9), A58–A56 (2009).
8. J. Nishizawa, T. Sasaki, Y. Oyama, and T. Tanabe, "Aspects of point defects in coherent terahertz-wave spectroscopy," Phys. B (Amsterdam, Neth.) **401-402**, 677–681 (2007).
9. H. Dezaki, T. Tanabe, J. Haiyan, and Y. Oyama, "Wide Frequency Tunable GaSe Terahertz Emitter under Collinear Phase Matching Condition," Key Eng. Mater. **500**, 58–61 (2012).
10. A. Kasuya, Y. Sasaki, S. Hashimoto, Y. Nishina, and H. Iwasaki, "Stacking fault density and splitting of exciton states in ε-GaSe," Solid State Commun. **55**(1), 63–66 (1985).
11. F. London, "The general theory of molecular forces," Trans. Faraday Soc. **33**, 8b (1937).
12. T. Tanabe, S. Zhao, Y. Sato, and Y. Oyama, "Effect of adding Te to layered GaSe crystals to increase the van der Waals bonding force," J. Appl. Phys. **122**(16), 165105 (2017).
13. J. Guo, D. J. Li, J. J. Xie, L. M. Zhang, Z. S. Feng, Y. M. Andreev, K. A. Kokh, G. V. Lanskii, A. I. Potekaev, A. V. Shaiduko, and V. A. Svetlichnyi, "Limiting pump intensity for sulfur-doped gallium selenide crystals," Laser Phys. Lett. **11**(5), 055401 (2014).
14. K. A. Kokh, J. F. Molloy, M. Naftaly, Y. M. Andreev, V. A. Svetlichnyi, G. V. Lanskii, I. N. Lapin, T. I. Izaak, and A. E. Kokh, "Growth and optical properties of solid solution crystals GaSe$_{1-x}$S$_x$," Mater. Chem. Phys. **154**, 152–157 (2015).
15. S. Zhao, Y. Sato, K. Maeda, T. Tanabe, H. Ohtani, and Y. Oyama, "Liquid phase growth of GaSe$_{1-x}$Te$_x$ mixed crystals by temperature difference method under controlled vapor pressure," J. Cryst. Growth **467**, 107–110 (2017).
16. S. A. Ku, W. C. Chu, C. W. Luo, Y. M. Andreev, G. Lanskii, A. Shaidukoi, T. Izaak, V. Svetlichnyi, K. H. Wu, and T. Kobayashi, "Optimal Te-doping in GaSe for non-linear applications," Opt. Express **20**(5), 5029–5037 (2012).
17. J. Guo, J. J. Xie, L. M. Zhang, D. J. Li, G. L. Yang, Y. M. Andreev, K. A. Kokh, G. V. Lanskii, A. V. Shabalina, A. V. Shaiduko, and V. A. Svetlichnyi, "Characterization of Bridgman grown GaSe:Al crystals," CrystEngComm **15**(32), 6323–6328 (2013).

18. Y. K. Hsu, W. C. Chen, J. Y. Huang, C. L. Pan, J. Y. Zhang, and C. S. Chang, "Erbium doped GaSe crystal for mid-IR applications," Opt. Express **14**(12), 5484–5491 (2006).

19. N. Lei, Y. Sato, T. Tanabe, K. Maeda, and Y. Oyama, "Transition metal doping of GaSe implemented with low temperature liquid phase growth," J. Cryst. Growth **460**, 94–97 (2017).

20. Y. Sato, C. Tang, K. Watanabe, T. Tanabe, and Y. Oyama, "Characteristics of 2D Ge-doped GaSe grown by low temperature liquid phase deposition under a controlled Se vapor pressure," J. Nanosci. Curr. Res. **03**(02), 1000128 (2018).

21. J. Guo, J. J. Xie, D. J. Li, G. L. Yang, F. Chen, C. R. Wang, L. M. Zhang, Y. M. Andreev, K. A. Kokh, G. V. Lanskii, and V. A. Svetlichnyi, "Doped GaSe crystals for laser frequency conversion," Light: Sci. Appl. **4**(12), e362 (2015).

22. V. G. Voevodin, O. V. Voevodina, S. A. Bereznaya, Z. V. Korotchenko, A. N. Morozov, S. Y. Sarkisov, N. C. Fernelius, and J. T. Goldstein, "Large single crystals of gallium selenide: growing, doping by In and characterization," Opt. Mater. **26**(4), 495–499 (2004).

23. Z. S. Feng, Z. H. Kang, F. G. Wu, J. Y. Gao, Y. Jiang, H. Z. Zhang, Y. M. Andreev, G. V. Lanskii, V. V. Atuchin, and T. A. Gavrilova, "SHG in doped GaSe:In crystals," Opt. Express **16**(13), 9978–9985 (2008).

24. D. R. Suhre, N. B. Singh, V. Balakrishna, N. C. Fernelius, and F. K. Hopkins, "Improved crystal quality and harmonic generation in GaSe doped with indium," Opt. Lett. **22**(11), 775–777 (1997).

25. Y. Sato, C. Tang, K. Watanabe, J. Ohsaki, T. Yamamoto, N. Tezuka, T. Tanabe, and Y. Oyama, "Terahertz wave generation via difference frequency generation by using 2D In$_x$Ga$_{1-x}$Se crystal grown from an indium flux," Opt. Express **28**(1), 472–477 (2020).

26. S. Das, C. Ghosh, S. Gangopadhyay, U. Chatterjee, G. C. Bhar, V. G. Voevodin, and O. G. Voevodina, "Tunable coherent infrared source from 5–16 µm based on difference-frequency mixing in an indium-doped GaSe crystal," J. Opt. Soc. Am. B **23**(2), 282–288 (2006).

27. O. Madelung, *Semiconductors: Data Handbook*, 3rd ed.; (Springer, Berlin, 2004) p. 524 & p. 531.

28. Y. Sato, C. Tang, K. Watanabe, M. Nakajima, T. Yamamoto, N. Tezuka, T. Tanabe, and Y. Oyama, "Optical and electrical properties of InxGa1-xSe mixed crystal grown from indium flux by the traveling heater method," *J. Electron. Mater.*, (Submitted)

29. R. L. Aggarwal and B. Lax, *1977 Nonlinear Infrared Generation*. Springer, New York, p. 28 (1977).

30. W. Shi, Y. J. Ding, X. Mu, and N. Fernelius, "Tunable and coherent nanosecond radiation in the range of 2.7–28.7 mm based on difference-frequency generation in gallium selenide," Appl. Phys. Lett. **80**(21), 3889–3891 (2002).